

CONTINUOUS WELDED RAIL IN CURVES OF SMALL RADII

Ludmila Chudějová^{*1}, Otto Plášek¹, Klára Murínová¹, Kateřina Koudelová¹, Michal Jedlička²

*ludmila.chudejova@vutbr.cz

¹Institute of Railway Structures and Constructions, Faculty of Civil Engineering, Brno University of Technology, Veveří 331/95, 602 00 Brno

²Institute of Structural Mechanics, Faculty of Civil Engineering, Brno University of Technology, Veveří 331/95, 602 00 Brno

Abstract

This paper provides a comprehensive review of the theory of continuous welded rail (CWR) mechanics and summarizes research results published to date with a focus on the stability of continuous welded rail. Axial forces arise mainly due to temperature changes and can cause rail crack in low winter temperatures or track buckling in high summer temperatures. The results of static analyses of the stability of CWR for small radii are presented.

Reduced stability is typical of curves of small radius ($R < 300$ m) where the lateral resistance of the track and the bending stiffness are exceeded. In curves of very small radii, lateral displacements of the track have been observed which reduce the axial forces in the track and thus reduce the risk of track buckling.

Keywords

Continuous welded rail, stability of continuous welded rail, track buckling, small radius directional curves

1 INTRODUCTION

Rail transport, with two centuries of history, maintains its significant role in the global transportation system. Despite the gradual impact of automotive and air transport competition, railway transport is still important due to a key element in the context of sustainable development and the reduction of CO₂ emissions. With rising oil prices and limited capacity of air and road transportation, the railway sector is becoming increasingly crucial for the future. To achieve successful development, it is essential to continuously improve the railway system, especially in terms of track and infrastructure, to meet the speed, safety and environmental standards.

One of the weakest elements of the railway line structure is the rail joint, especially in terms of maintenance, reliability and ride comfort. Efforts to improve it have led to its elimination, and about 100 years ago, the CWR was introduced. Focusing on the specific aspects of the CWR, an important question arises concerning the stability of directional curves with a small radius ($R < 300$ m), especially in the warm summer months when the risk of rail buckling can occur.

This study attempts to elucidate this issue using numerical models, aiming to better understand the behavior of the railway track under challenging conditions. The research investigates the influence of various parameters of construction and loading, such as curve radius, rail section, lateral resistance of the track ballast, temperature, and braking and starting forces from vehicles on track stability. Fig. 1 shows a block diagram of these factors. In this way, it seeks to contribute to the reliability and sustainability of railway transportation in the future.

The purpose of this article is to summarize the current knowledge on CWR stability and the results of static analyses of CWR stability published in previous master's theses.

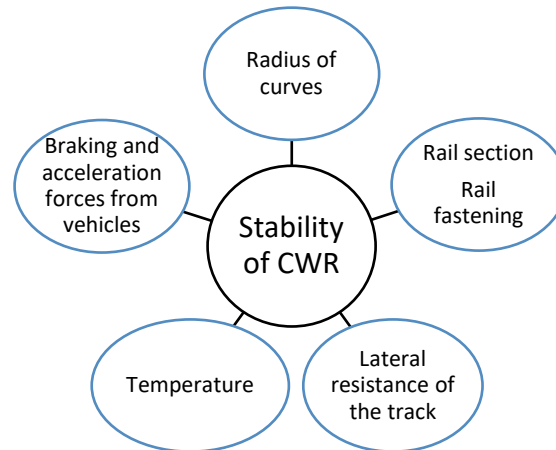


Fig. 1 Block diagram of the influence factors on the CWR stability.

Theory of Continuous Welded Rail

CWR is a type of construction where the rails and turnouts are connected through welding. In CWR, after welding, axial forces are generated due to temperature changes relative to the neutral temperature. These axial forces can negatively impact the stability of the rail and lead to CWR malfunctions. These malfunctions can result in rail crack (in low temperatures during the winter) and/or in a more serious loss of rail stability (in high temperatures). The loss of stability often leads to subsequent track buckling, manifesting in either vertical or horizontal displacements.

The physical principle of thermal expansion of the material when the temperature changes applies to a free-lying rail equation (1):

$$\pm \Delta l = \alpha \cdot l \cdot (t - t_0) \quad (1)$$

where l is the length of the rail in m, Δl is the extension or shortening of the rail length due to temperature in m, α is the coefficient of thermal expansion in $^{\circ}\text{C}^{-1}$, t is the actual rail temperature in $^{\circ}\text{C}$ and t_0 is the neutral temperature in $^{\circ}\text{C}$.

The neutral temperature is the temperature at which the axial force of the CWR is zero. During the establishment of CWR (welding rails into CWR), the neutral temperature equals the clamping temperature. By clamping the rails to sleepers/supports, the longitudinal resistance of the track is activated. To elongate the rail segments according to the formula (1), it is necessary to overcome the longitudinal resistance first, consisting of the resistance in fastening (7 kN per fastening node [1]) and the resistance of the track ballast (10 kN per 1 meter of track [1]).

The axial force in the installed rail segment generates stress in the rail. If the temperature rises above the neutral temperature during the construction, it results in compressive stress, whereas if the temperature drops below the clamping temperature, it leads to tensile stress. Stress σ can be expressed by the well-known equation (2):

$$\sigma = \frac{N}{A} \quad (2)$$

where A is the area of the rails in m^2 .

Based on the Hooke's law for the force N acting against the elongation of the rail, the following equation can be formulated (3):

$$\Delta l = \frac{\sigma \cdot l}{E} = \frac{N \cdot l}{E \cdot A} \quad (3)$$

where E is the elasticity modulus of rail steel in Pa.

When comparing formulas (1) and (3), we obtain the relationship for stress during temperature change (4):

$$\sigma = \alpha \cdot E \cdot (t - t_0) \quad (4)$$

In the conditions of the Czech Republic, temperatures are considered in the range from -30°C to $+60^{\circ}\text{C}$. This means that at a neutral temperature of $+20^{\circ}\text{C}$, there is an increase in tensile stress of 126 MPa and in compressive stress of 101 MPa.

The CWR is considered to be a track with a length of at least 150 m [1]. The CWR consists of a breathing end and a middle section, with the length of the breathing end considered to be 75 m. This length was determined with regard to the most unfavorable values of longitudinal resistance and temperature differences. At the breathing end, dilation movement can occur during temperature changes (after overcoming the resistance in the joint establishing the dilation gap). However, in the middle section, dilation movement cannot occur because it is hindered by the longitudinal resistance of the track structure. Therefore, the CWR can have two breathing ends and a middle section or two breathing ends.

Theory of Axial Forces

For the substitute rail element in Fig. 2, we can formulate the equilibrium equation (5).

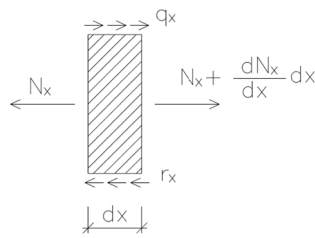


Fig. 2 Substitute rail element in the longitudinal direction.

$$-N_x + N_x + \frac{dN_x}{dx} dx + q_x \cdot dx - r_x \cdot dx = 0 \quad (5)$$

This equation can be modified into the following equation (6):

$$\frac{dN_x}{dx} = r_x - q_x \quad (6)$$

where r_x is the longitudinal resistance, q_x is the braking and acceleration loads.

Based on the knowledge on the deformation relationship, we can write the equation (7):

$$\varepsilon = \frac{\sigma}{E} = \frac{N_x}{EA}; \quad \varepsilon = \frac{du}{dx} - \alpha \cdot (t - t_0) \quad (7)$$

where u is the displacement of the rail cross-section in m.

By substituting the equation (7) into the equation (6), the basic differential equation (8) is obtained:

$$\frac{d^2u}{dx^2} EA - r_x = 0 \quad (8)$$

The load q_x is neglected in the calculation.

The calculation is significantly influenced by the function of the longitudinal resistance r_x , which, in this case, has been simplified into an equation as follows (9):

$$r_x = -r_0 \cdot \text{sign}(t - t_0) \quad (9)$$

where r_0 is value of the longitudinal resistance in N.

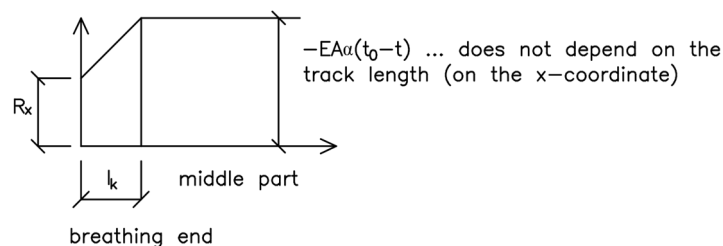


Fig. 3 Distribution of axial forces along the length of the rail.

The length of the breathing end can be obtained from the knowledge of the distribution of axial forces along the length of the rail in Fig. 3. Hence the equation (10):

$$R_x + \int_0^{l_k} r_x \cdot dx = -EA \cdot \alpha \cdot (t - t_0) \quad (10)$$

By integrating and adjusting equation (10), we obtain the expression for the length of the breathing end in equation (11):

$$l_k = \frac{-R_x - EA \cdot \alpha \cdot (t - t_0)}{r_x} \quad (11)$$

Derivation of equation (8) gives the basic equation (12) for the displacement u at the breathing end:

$$u = \frac{r_x \cdot x^2}{2EA} + C_1 x + C_2 \quad (12)$$

Boundary conditions in equations (13) and (14):

$$u(l_k) = 0 \quad (13)$$

$$R_x = EA \cdot \varepsilon(0) = EA \left(\frac{du}{dx}(0) - \alpha \cdot (t - t_0) \right) = -R_0 \cdot \text{sign}(t - t_0) \quad (14)$$

where R_x is the axial force at the end of CWR in N and R_0 is the value of axial force at the end of CWR in N.

Substituting the boundary conditions (13) and (14) into the equation (12), we obtain the formula for the track displacement at the breathing end, equation (15):

$$u = \frac{r_x}{2EA} (x - l_k)^2 \quad (15)$$

Stability of Continuous Welded Rail

The stability of CWR is a crucial indicator of the reliability of railway operations. The stability of CWR is primarily influenced by temperature changes in relation to the neutral temperature. When the rail temperature rises above the neutral temperature, longitudinal compressive forces are generated due to the prevention of rail expansion. This results in stress in the rail, affecting the stability of CWR. In addition to temperature effects, dynamic loading also plays a role, as it can destabilize the rails and disrupt their equilibrium.

If passive forces are overcome, track buckling may occur. Track buckling can manifest as a deformation in the horizontal or vertical direction (most commonly, deformation occurs in both directions simultaneously). The process of track buckling can occur gradually in several phases. It begins with the lifting of the track, leading to a reduction in the lateral resistances of the track structure in the track ballast. The decrease in resistances eventually allows the track to buckle in the transverse direction.

The longitudinal and lateral resistances are crucial for the stability of CWR. Longitudinal resistance consists of the resistance at the attached node and the resistance of the sleeper in the longitudinal direction, as mentioned earlier. Lateral resistance depends on the resistance of the sleeper in the transverse direction in the track ballast, the weight of the sleeper, the type of rails, and the overall frame stiffness of the track structure.

The resistance of the sleeper in the transverse direction is influenced by the friction of the bearing surface and the lateral sides of the sleeper on the track ballast, as well as the amount of material in the track ballast behind the head of the sleeper. The sleeper resistance can be proportionally divided as follows:

- 45% friction of the sleeper's bearing surface on the track ballast,
- 35% friction of the lateral sides of the sleeper on the track ballast,
- 20% resistance of the track ballast behind the head of the sleeper [2].

It can be argued that sleepers that are not rectangular, especially those that are transverse or shaped in the middle, have significantly higher lateral resistance. The quality and consolidation of the ballast bed plays a decisive role in the lateral resistance of the sleeper. On heavily loaded lines, consolidation of the track ballast can occur within a few days, but on lightly loaded lines, consolidation can take a very long time. It should be noted that on less heavily loaded lines, directional curves with small radii are often present, and for example, insufficient track fill can interfere with consolidation.

The weight of the sleepers used in the track is an important parameter in track design that affects the stability of the track. The heavier the sleeper, the higher the stability of the CWR.

The bending stiffness of the track structure depends on the moment of inertia of the rails about an axis perpendicular to the track structure, the sleepers and their distribution, the rail attached, and the modulus of elasticity of the steel. It can be said that the greater the value of the moment of inertia, the greater the bending stiffness of the track. However, it is essential to remember that an increasing value of the moment of inertia leads to an increase in the cross-sectional area of the rails and thus the acting axial force.

The bending stiffness of the track structure plays a significant role in both the horizontal and vertical planes. In the vertical plane, stiffness can be calculated similarly to the rail (individual sleepers do not contribute to the stiffness), while in the horizontal plane, the influence of sleepers and stiffness in fastening must be taken into account.

Another important parameter influencing the stability of the track is the initial lateral displacement, as shown in Fig. 4.

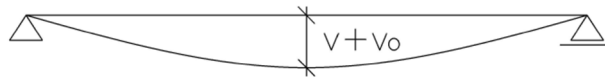


Fig. 4 Overall lateral displacement.

Fig. 5 illustrates the internal forces acting on the track's substitute member element, where the axial force in the buckling zone is constant.

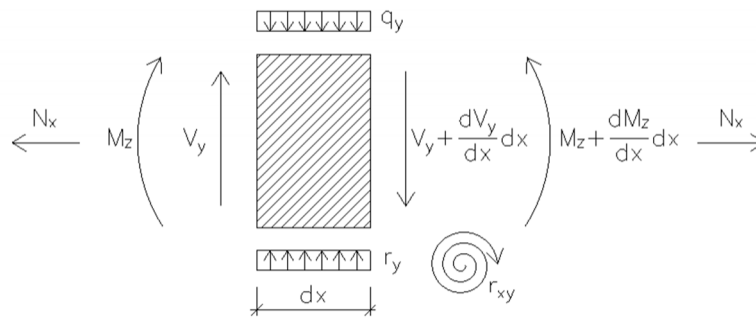


Fig. 5 Substitute member element of the track in the lateral direction.

From Fig. 5, we can determine the bending moment M_z acting on the track structure, as shown in equation (16):

$$M_z = M_z^{(1)} + M_z^{(2)} = M_z^{(1)} \pm N_x \cdot (v + v_0) = -EI_z \cdot \frac{d^2v}{dx^2} \pm N_x \cdot (v + v_0) \quad (16)$$

where v is the lateral displacement function in m, v_0 is the initial lateral displacement function in m and I_z is the moment of inertia of the track (2 rails + sleepers + stiffness in the attached node) in m^4 .

The balance of forces and moments can be expressed as follows, in equations (17) and (18):

$$dV_y + q_y \cdot dx - r_y \cdot dx = 0 \quad (17)$$

$$dM_z - 2V_y \cdot \frac{dx}{2} - r_{xy} \cdot dx = 0 \quad (18)$$

By adjusting equations (17) and (18), we obtain the equation (19) for lateral resistance:

$$\frac{d^2M_z}{dx^2} = \frac{dV_y}{dx} + \frac{dr_{xy}}{dx} = r_y - q_y + \frac{dr_{xy}}{dx} \quad (19)$$

where r_y is the function for lateral resistance, r_{xy} is the function for torsional stiffness of the attached node and q_y is the lateral continuous load.

If we derive the equation (16) twice and substitute it into the equation (19), we obtain the basic differential equation (20) under the assumption that the axial force N_x is constant, and we do not consider the initial imperfection v_0 :

$$-EI_z \cdot \frac{d^4 v}{dx^4} \pm N_x \frac{d^2 v}{dx^2} = r_y - q_y + \frac{dr_{xy}}{dx} \quad (20)$$

For double-ended member with rigid support member with elastic restrain, we consider four boundary conditions, as can be seen from quations (21), (22), (23) and (24):

$$v(0) = 0 \quad (21)$$

$$v(L) = 0 \quad (22)$$

$$\frac{dv}{dx}(0) = 0 \quad (23)$$

$$\frac{dv}{dx}(L) = 0 \quad (24)$$

The lateral resistance at the point of buckling is considered constant, where both the displacement and the lateral resistance are zero. The assumed value of the lateral resistance is $r_0 = 7$ kN/m for a track with concrete sleepers, and this value already includes dynamic effects. The calculation neglected the torsional stiffness in the fastening r_{xy} and the lateral continuous load q_y .

The dependence of the lateral resistance on the lateral displacement is determined by the equation (25):

$$\begin{aligned} r_y &= k \cdot v \\ k &= \frac{r_0}{v_0} \end{aligned} \quad (25)$$

By substituting into equation (20), we obtain the equation (26):

$$EI_z \cdot \frac{d^4 v}{dx^4} \mp N_x \frac{d^2 v}{dx^2} + k \cdot v = 0 \quad (26)$$

By successive adjustments, we obtain nontrivial solutions for the critical force N_{krit} , the critical length L_{krit} , and critical temperature increase ΔT_{krit} , in equations (27), (28) and (29):

$$N_{krit} = \frac{n^2 \pi^2}{L^2} \cdot EI_z + \frac{k \cdot L^2}{n^2 \pi^2} \quad (27)$$

$$L_{krit} = \sqrt[4]{\frac{EI_z}{k}} \cdot n \cdot \pi \quad (28)$$

$$\Delta T_{krit} = \frac{N_{krit}}{\alpha \cdot EA} \quad (29)$$

where L is the length of wave in m and n is constant.

It can be proven that the critical axial force N_{krit} is the smallest for $n_{krit} = 1$. Subsequent editing of the formula and substitution of the formula for the critical length L_{krit} reveals again that the critical constant n_{krit} equals 1.

By substituting formula (28) into formula (27), we obtain the final expression for the critical force N_{krit} , in the equation (30):

$$N_{krit} = 2\sqrt{k \cdot EI_z} \quad (30)$$

According to Lichtberg [3], the equations determining the critical axial force N_{krit} and the critical length L_{krit} as functions of the initial lateral deflection v_0 and lateral resistance r_0 are as follows in equations (31) and (32):

$$N_{krit} = 2,96 \cdot \sqrt{\frac{EI_z \cdot r_0}{v_0}} = 177 \cdot \frac{EI_z}{L_{krit}^2} \quad (31)$$

$$L_{krit} = 7,75 \sqrt[4]{\frac{EI_z \cdot v_0}{r_0}} \quad (32)$$

The theory mentioned above is established only for a straight track. The stability issue must be addressed in a directional curve, as it is especially directional curves with small radii that are prone to track buckling.

To formulate formulas for a track in a curve, it is necessary to introduce polar coordinates. Here, R represents the constant radius of the directional curve (radial coordinate), and θ is the tangential coordinate. We will transform the equilibrium equation (20) into polar coordinates in the following equations (33):

$$-\frac{EI_z}{R^4} \cdot \frac{d^4 v}{d\theta^4} \pm \frac{N_\theta}{R^2} \frac{d^2(v + v_0)}{d\theta^2} - \frac{N_\theta}{R} = r_r - q_r + \frac{dr_{\theta R}}{d\theta} \quad (33)$$

where r_r is function $r_{r(v)}$ of lateral resistance in N/m, $r_{\theta R}$ is the function $r_{\theta R}(\frac{dv}{d\theta})$ of torsional stiffness and q_r is the lateral continuous load.

The final equations for the critical force N_{krit} and the critical length L_{krit} for a curved track are as follows in equations (34) and (35):

$$N_{krit} = \frac{-8EI_z}{v_0 \cdot R} + \sqrt{\left(\frac{8EI_z}{v_0 \cdot R}\right)^2 + \frac{16EI_z \cdot r_o}{v_0}} \quad (34)$$

$$L_{krit} = 2\pi \sqrt{\frac{2EI_z}{N_{krit}}} \quad (35)$$

The theory described above clearly shows that the initial imperfection has a crucial influence on track buckling. The curvature of the track radius also plays a significant role; the smaller the radius, the lower the lateral resistance of the track structure, resulting in decreased stability of the CWR.

Track breathing in horizontal curves

Another influence on the stability of CWR is the lateral movement, the so-called "breathing of the track," which occurs in sections with horizontal curves during temperature changes. This movement leads to a reduction in the axial force in CWR and results in a change in neutral temperature ΔT_N , as shown in the equation (36):

$$\Delta T_N = \frac{v_e}{R \cdot \alpha} \quad (36)$$

where ΔT_N is the change in neutral temperature in °C and v_e is the lateral displacement of the track from the center of the curve in m.

Track breathing was observed in Switzerland between 2011–2013 [4], where the behavior of CWR was monitored over an extended period on four sections of a narrow-gauge track with radii of approximately 100 m. Data on rail temperature, air temperature, changes in rail stress, and the lateral displacement of the track were recorded. Sensors were also installed to detect train passages. Along the monitored section, there were fifteen measurement points where individual values were recorded.

As part of the evaluation, a linear dependence of lateral displacements on the radius size was observed. However, lateral displacements did not develop uniformly along the length of the curve; instead, small waves were formed. In Fig. 6, the course of lateral displacements over time and rail temperature are shown. Train passages are indicated by the vertical lines. It can be noticed that larger displacements occur abruptly with the passage of railway vehicles. This phenomenon is caused by the reduction in transverse resistance when the sleepers are lifted as the train passes and the vibration from the train passing itself, with the combination of increasing stress in the rail from increasing temperature.

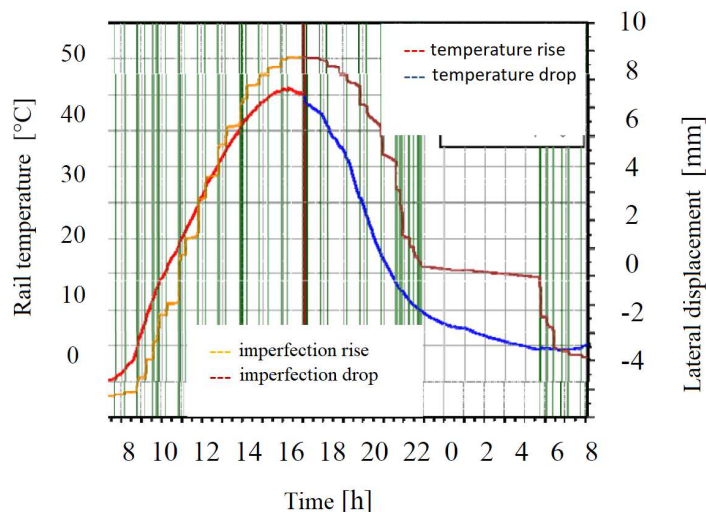


Fig. 6 Time course of temperature and lateral displacement [4].

In conclusion, the emphasis was put on paying greater attention to several key issues. The first aspect is maintaining uniform lateral resistance throughout the entire length of the track, which helps prevent the formation of areas with excessive or insufficient resistance effects. There was also a focus on a thorough control of the track's alignment during its installation. Finally, it was recommended to carry out track tamping at a neutral temperature [4].

2 RAIL TRACK MODEL IN A DIRECTIONAL CURVE

In the master's thesis by Ing. Peřinová [5], a numerical model was created using the Dlubal RFEM 5.08 software, which computed results only linearly. Conversely, in the master's thesis by Ing. Murínová [6], a model was created using the Ansys Classic v. 19.2. – Mechanical APDL software, which eliminated the limitations of the RFEM program and computed results nonlinearly. Subsequently, the results obtained using the software with nonlinear calculations will be presented.

The basis for the model was the creation of the geometry of the curved track. The length of the observed curve was 60 m, and the neutral rail temperature was set to 20 °C (within the allowable clamping temperature range). An initial imperfection was created since it is apparent from the conclusions presented in Ing. Peřinová's master's thesis [5] that curved tracks without initial imperfections do not provide realistic results. The initial imperfection has a sinusoidal shape and is located in the middle of the section. The length of the wave was chosen to be 17 m, and the maximum deflection was set to 10 mm. Calculations were performed for three different radius values: 300 m, 225 m, and 150 m. For these radii, the recommended track superelevation [7] and, for curves with a radius R less than 275 m, the gauge widening [7] was calculated.

The sleepers were considered type B 91S and their model was simplified to a plain rectangular prism without the typical shape of these sleepers, while the total mass was preserved. For this model, the BEAM 188 element was used, with six to seven degrees of freedom.

Individual calculations were also divided according to the shape of the rails used, considering rails 49 E1 and 60 E2 with steel R260. For their model, the BEAM 189 element was used, which has one additional node compared to the BEAM 188 element and captures the rail and its potential bending better.

The anchoring node was modeled using the COMBIN 14 element, representing a flexible element with damping capabilities. The connection between the rail and the sleeper was modeled with four COMBIN 14 elements, three representing stiffness in the X, Y, and Z axes, and the last representing the torsional stiffness of the anchoring node around the Z axis.

The lateral resistance was defined using the COMBIN 39 element, which is a nonlinear element without mass or thermal capacity. The element was defined by a curve representing the relationship between deformation and force, as shown in Fig. 7.

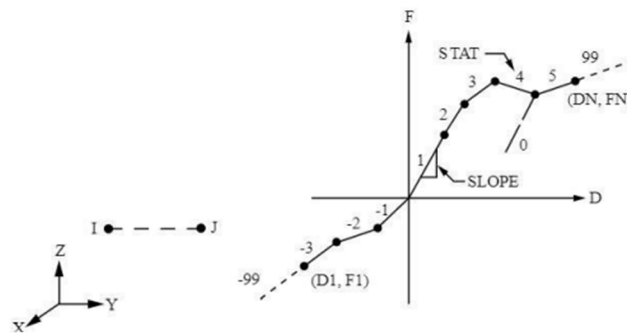


Fig. 7: The curve of the dependence of the deformation on the force defining the element [8].

The stiffness of the track ballast is defined using the same element as the rail anchoring, COMBIN 14, which represents the stiffness of the track ballast against displacement in the Z-axis. The value is derived from a volumetric stiffness of 0.3 N/mm^3 .

Loading was considered only in terms of temperature and the self-weight of the components. Temperature was applied only to elements representing the rails.

3 RESULTS

The loading process proceeded gradually with changing temperatures, ranging from $-30 \text{ }^\circ\text{C}$ to $+80 \text{ }^\circ\text{C}$, and then back to $-30 \text{ }^\circ\text{C}$, repeating the cycle. This was done in increments of $10 \text{ }^\circ\text{C}$ starting from the initial temperature of $20 \text{ }^\circ\text{C}$. The entire cycle was performed in 45 loading states for curvature radii of 300 m and 225 m. For a curvature radius of 150 m, only the first 24 loading states were simulated, due to convergence issues in the model. This comprehensive loading cycle simulates the alternating seasons throughout the year.

Shape of Track Buckling

On the model subjected to the entire loading cycle, we can observe the developed shape of track buckling which consists of three half-waves of symmetric shape. A similar deformation curve can be observed for all models. In Fig. 8, the shape of lateral track buckling captured at various positive temperatures within the loading cycle is shown. It can be noticed that, for the rail of type 60 E2, larger lateral displacements occur compared to the rail of type 49 E1. Additionally, the model with the 60 E2 rail has a greater lateral displacement between the first and second cycles. As a result, the buckling curves do not overlap as much as in the case of the 49 E1 rail. Similar results can be observed for negative temperature values.

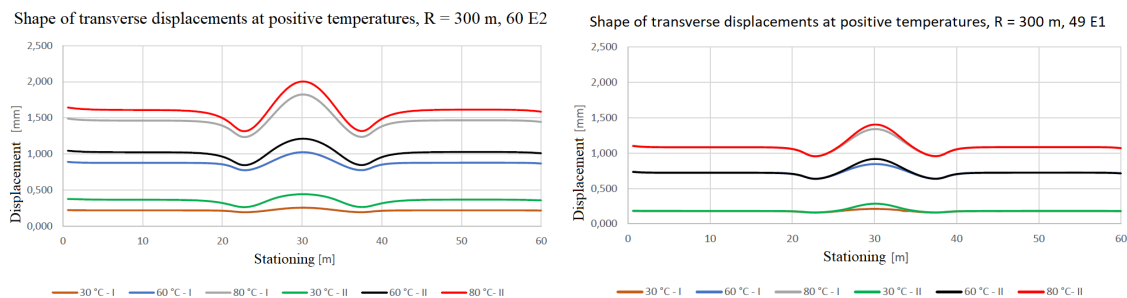


Fig. 8 The shape of the lateral track deviation for a radius of $R = 300 \text{ m}$ and rail sections 60 E2 and 49 E1 [6].

In Fig. 8, an ideal curve with three symmetrical half-waves along the y-axis can be observed; however, not all models exhibited this result. Generally, symmetrical curves were observed in the case of models with rail section 49 E1, while less symmetrical results were recorded for the model with rail section 60 E2 and a radius of curvature $R = 225 \text{ m}$. This unexpected outcome may signal inadequate problem formulation or numerical method instability where inaccuracies in the results could be caused by a small error, especially rounding, in the input data values. For comparison, Fig. 9 shows graphs of lateral displacements for individual radii and rail sections under a temperature load of $80 \text{ }^\circ\text{C}$.

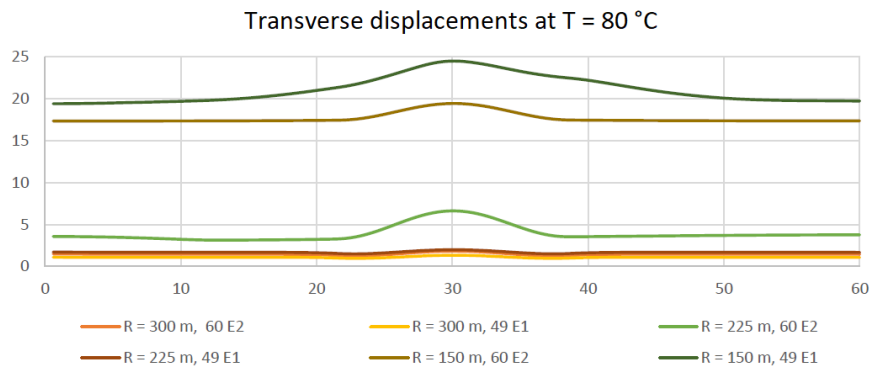


Fig. 9 Shape of lateral deviation for $R = 300$ m and rail sections 60 E2 and 49 E1 [6].

Course of the track heating and cooling cycle

The main intention was to identify the response of CWR to the complete heating and cooling cycle. To display the lateral displacement in relation to loading, the central part of the model in the middle of the formed wave, where the values of lateral displacement reach maximum values, was selected.

From Fig. 10, the course of the entire heating and cooling cycle back to the original clamping temperature can be observed. This graph is plotted for a radius of $R = 150$ m, where the course of lateral displacements is nonlinear. Conversely, for a radius of $R = 300$ m, the lateral displacement graph turned out to be linear with values of lateral displacements more than ten times smaller.

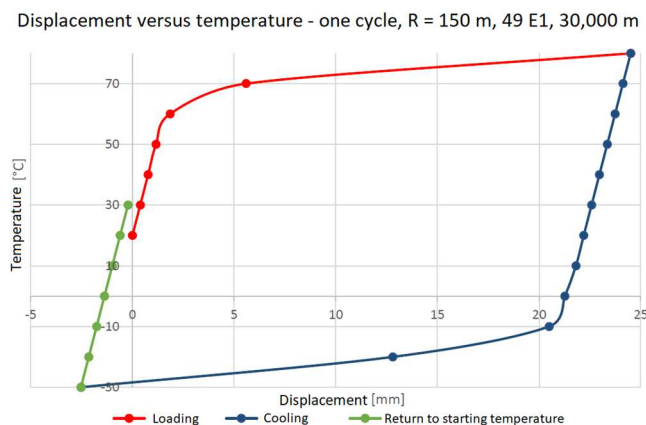


Fig. 10 Course of lateral displacements in one load cycle for $R = 150$ m [6].

The course of the cooling and warming cycle of the track

The establishment of the CWR at a certain time of year is critical. If the CWR were to be established in the autumn, the first cycle would not be a warming but a cooling. In Fig. 11, the progression of lateral displacements for one cycle is depicted, with cooling of the track occurring as the first step. In comparison to Fig. 10, a significant change in the values of lateral displacements for the same track model can be observed, as well as the fact that the values do not return to their initial position.

Displacement versus temperature - one cycle, R = 150 m, 49 E1, 30,000 m

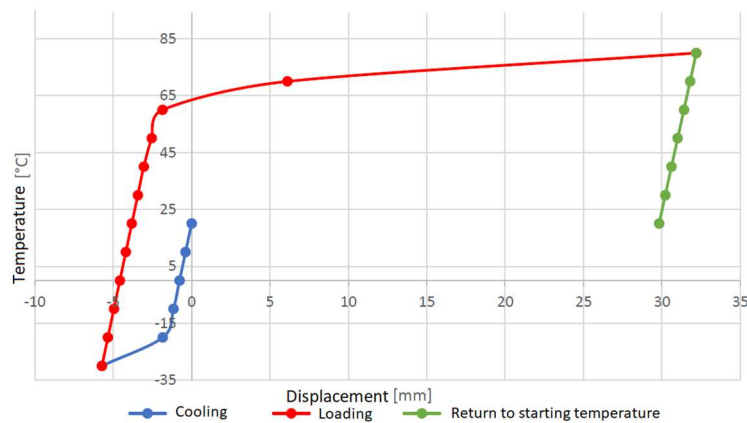


Fig. 11 Progression of lateral displacements in one loading cycle for R = 150 m [6].

4 DISCUSSION

The presented results indicate that directional curves with a smaller radius exhibit larger lateral displacements than those with larger radii. Additionally, rail type 60 E2 shows greater lateral displacements than rail type 49 E1. During the heating and cooling cycles of the track, the track structure returns almost to its original position after lateral displacements at the end of the cycle. However, if the cycle begins with cooling, the track does not return to its original position at the end of the cycle. This fact is crucial because, during subsequent cycles of cooling and heating, the track would again show larger lateral displacements at the end of the cycle.

An initial deflection of 10 mm was introduced into the model to represent a possible imperfection in the track, which may develop into a track buckling. The value was chosen outside the range of operational deviations in the Immediate Action Limit (IAL) [9], so it could be said that once the deflection reaches a value above the IAL, it can be considered as a track buckling.

The theoretical analysis provides basic information about the behaviour of contactless track and with regard to simplification, its use in small radius curves is inappropriate. Direct comparison of the results with numerical analyses is not possible. In view of the complexity of the problem, this comparison will be the subject of further theoretical work.

5 CONCLUSIONS

This article summarizes the theory of the stability of CWR and the results obtained from previous master's theses. Numerical models were created in the Ansys Classic program version 19.2 – Mechanical APDL for three different radii of directional curves and two basic rail sections. The models were subjected to temperature loads, and a total of 45 loading states were created to simulate a loading cycle that mimics the changing seasons.

A difference was observed in lateral displacements and internal forces in the track with rail sections 49 E1 and 60 E2. It can be assumed that due to the different cross-sectional characteristics, there is a variation in force distribution, resulting in differences in the final values. Exceeding the critical temperature could lead to track buckling at the point of maximum displacement.

The graphs of the loading cycle for smaller radii (Fig. 9 and 10) show a nonlinear increase in lateral displacements caused by the plastic behavior of the lateral resistance of the environment in which the track is located upon reaching a certain lateral displacement. For a larger radius, the cycle graph approaches a linear relationship, meaning the track resistance moves in a linear branch, where the lateral displacement value does not exceed 2–3 mm. No track model returned to its original position within the completion of the cycle, residual lateral displacements always remain in the track. As the radius of the track curve decreases, the residual displacement increases. Reversing the cycle to cooling and subsequent heating significantly increased the residual displacement value. This should be the subject of further investigation.

Continuing the study of track stability could involve refining the basic track model, including determining the real behavior of lateral resistance of the sleeper in actual conditions and studying the track in daily cycles.

Another subject for investigation could be tracking the breathing in horizontal curves with small radii and conditions corresponding to real conditions.

References

- [1] SŽDC s.o: Předpis SŽDC S3/2 Bezstyková kolej. Approved by the Director General SŽDC on 24 May 2013 under no.: S11167/2013-OTH, effective from 1. September 2013
- [2] ZVĚŘINA, Pavel. Železniční stavby: Návody do cvičení II. Brno, Brno University of Technology, 1989
- [3] LICHTBERGER, Bernhard. Track compendium: track system, substructure, maintenance, economics. 2nd edition, completely revised. Hamburg: DVV Media Group GmbH Eurailpress, 2011. ISBN 978-3-7771-0421-8.
- [4] SCHNEIDER, Philippe. UIC Projekt "USP in track": WP 2: Lateral Track Stability. SBB CFF FFS. 2011, 2011(06), 24.
- [5] Peřinová, K. (2018). Bezstyková kolej v obloucích malých poloměrů. *Dspace.vut.cz*. Available at: <http://hdl.handle.net/11012/70754> (accessed 2023-11-15)
- [6] Murínová, K. (2021). Nelineární analýza bezstykové koleje v obloucích malého poloměru. *Dspace.vut.cz*. Available at: <http://hdl.handle.net/11012/196008> (accessed 2023-11-15)
- [7] ČSN 73 6360-1. Geometrical characteristics of railway tracks – Part 1: Layout, december 2020, 52 p. Prague: Czech Standards Institute, 2020.
- [8] ANSYS Help [online]. Canonsburg, PA: ANSYS, 2018 [accessed 2023-11-15]. Available at: <https://ansyshelp.ansys.com/>
- [9] ČSN 73 6360-2 Geometrical characteristics of railway tracks - Part 2: Construction and acceptance, service and maintenance. August 1997. Prague: Czech Standards Institute, 1997.